Ceramics International 51 (2025) 36637–36643

Contents lists available at ScienceDirect

Ceramics International

journal homepage: www.elsevier.com/locate/ceramint

# Magnesium whitlockite structure: an *ab initio* approach supported by experimental characterization

Emanuel Cleyton Macedo Lemos [a,b], Renata Hidemi Moriya [a], Luccas Correa Teruel de Jesus [a], Roger Borges [a,c], Rene Ramos de Oliveira [d], Nelson Batista de Lima [d], Jeverson Teodoro Arantes [e], Juliana Marchi [a,*]

[a] Centro de Ciências Naturais e Humanas (CCNH), Universidade Federal do ABC (UFABC), Santo André, SP, Brazil
[b] Departamento de Ensino, Instituto Federal do Maranhão (IFMA), Campus Santa Inês, MA, Brazil
[c] Escola de Engenharia Biomédica, Faculdade Israelita de Ciência das Saúde Albert Einstein, Hospital Israelita Albert Einstein, São Paulo, SP, Brazil
[d] Centro de Ciência e Tecnologia de Materiais (CCTM), Instituto de Pesquisas Energéticas e Nucleares (IPEN), São Paulo, SP, Brazil
[e] Centro de Engenharia e Ciências Sociais Aplicadas (CECS), Universidade Federal do ABC (UFABC), Santo André, SP, Brazil

ARTICLE INFO

Handling Editor: Dr P. Vincenzini

*Keywords:*
Whitlockite
Bioceramic
*Ab initio* method.

ABSTRACT

Magnesium whitlockite (Mg-WH), the second most abundant inorganic material in hard tissue, is a promising biomaterial and participates in cell signaling through piezoelectric modulation. However, its electric structure is not fully understood. This study investigated the structure and electronic structure of Mg-WH for the first time using *ab initio* methods. Additionally, Mg-WH was synthesized through the coprecipitation method and characterized by scanning electron microscopy (SEM-FEG), X-ray diffraction (XRD), and Fourier-transform infrared (FTIR) spectroscopy. The experimental results of XRD were compared with those obtained by computational simulation, and good agreement was shown. The Ca1 site of Mg-WH showed a higher distance between magnesium and other coordinated oxygens, making it more likely to accommodate atomic substitution in Mg-WH doping concerning elements with ionic radii bigger than $Mg^{2+}$. Besides, the theoretical model confirmed the presence of a hydrogen bond due to the presence of the $HPO_4^{2-}$ group at the Ca4 site, which was further confirmed by the experimental FTIR spectrum. This hydrogen bond and $Mg^{2+}$ in Mg-WH may play an essential role in physiological environments.

## 1. Introduction

Human bone tissue can recover from non-critical defects through the gradual process of osteogenesis mediated by osteoblast cells. However, its regenerative capacity may not be enough to rebuild the damaged tissue in severe injuries or under pathological conditions, like osteomyelitis and osteosarcoma [1–4]. Bone substitutes and biomaterials that aim to assist bone regeneration have been the subject of research for several years [5]. Some of the most studied materials include calcium phosphate phases, such as hydroxyapatite (HAp) and β-tricalcium phosphate (β-TCP), besides bioactive glasses, where all of them display high bioactivity, osteoconduction, and osteointegration potential [6]. Recently, magnesium whitlockite (Mg-WH), a calcium phosphate ceramic with the chemical formula $Ca_{18}Mg_2H_2(PO_4)_{14}$, has gained attention due to its potential applications in bone repair allied with low-intensity ultrasound therapy [7].

Whitlockite can be found in nature in three different forms: two inorganic and one of biological origin [8]. In the human body, it is found in bone tissue and dentin, representing the second most abundant inorganic mineral in hard tissue. Based on the amount of magnesium ions, their presence in bone minerals can be estimated at 20 %, and it is higher in the early stages of mineralization and young bones. Moreover, approximately 26–58 % of the whitlockite phase is present in human dentin [9]. Even though human bone serves as a reservoir of calcium ions (99 %) in the human body, mainly as HAp, magnesium ions are also significant, corresponding to approximately 50 %, in the form of Mg-WH [9,10].

Considering that magnesium ions play an essential role in the functioning of the human skeletal, nervous, and muscular systems, several studies have focused on doping HAp and β-TCP with $Mg^{2+}$ ions to enhance their biological properties [11–14].

Although synthetic hydroxyapatite closely resembles the inorganic

* Corresponding author.
*E-mail address:* juliana.marchi@ufabc.edu.br (J. Marchi).

https://doi.org/10.1016/j.ceramint.2025.05.374
Received 12 December 2024; Received in revised form 6 May 2025; Accepted 27 May 2025
Available online 30 May 2025

phase of bone and teeth, its resorption is lower due to its high stability under physiological conditions [15]. Among the various calcium phosphates, β-TCP is the second most used bioceramic in clinical practice. Its relatively high solubility and dissolution products stimulate bone formation through osteoblast signaling. However, the ability of β-TCP to bond to the bone tissue through a surface apatite layer, as HAp or bioactive glasses do, is still debated [16].

Whitlockite shares structural similarities with β-tricalcium phosphate, β-$(Ca_3PO_4)_2$, differing in the presence of $HPO_4^{2-}$, calcium substitutions for magnesium ions, and cation vacancies at the crystallographic calcium sites V and IV [8]. Whitlockite is biocompatible and displays potential bioactive behavior in hard tissues, enabling this biomaterial to induce bone regeneration like HAp and β-TCP implants [17]. Despite being a well-known biomaterial in the human body under physiological conditions, its detection by analytical techniques is challenging due to its short-range presence, resulting in limited research on Mg-WH as a biological material in the years before [9].

In contrast, new synthesis routes have sparked the development of works on synthetic Mg-WH in recent years. For instance, Jang et al. [9] synthesized whitlockite nanoparticles based on the ternary system $Ca(OH)_2$-$Mg(OH)_2$-$H_3PO_4$ under acidic pH conditions and limited excess of $Mg^{2+}$ to prevent hydroxyapatite formation or other undesired phases. Besides obtaining only whitlockite as a crystalline phase in the nanoparticles, the authors also demonstrated that whitlockite nanoparticles exhibit *in vitro* biocompatibility comparable to hydroxyapatite. Further evidence of the biocompatibility of Mg-WH was shown by Qi et al. [18], who reported a rapid microwave-assisted synthesis of single-phase hollow porous microspheres of Mg-WH. These microspheres also showed high biocompatibility and good adhesion of osteoblastic cells, demonstrating that cell biocompatibility occurs regardless of particle shape. Notwithstanding, not only can the biocompatibility of Mg-WH be explored in biomedical applications, but also its piezoelectric properties. Kaliannagounder et al. [15] highlighted the piezoelectric properties of Mg-WH as an enhancer for bone regeneration ability in the human body by aligning bioinorganic and mechanical stimuli on osteogenesis. It is worth noting that despite the piezoelectric properties of Mg-WH being known, its electronic structure is not fully understood.

The development of synthetic Mg-WH, coupled with computational simulation, has also promoted further elucidation of its morphology and structure — for example, Wang et al. [19] synthesized Mg-WH nanoplates using a tri-solvent system that controls their size, morphology, and surface properties. Through molecular dynamics (MD) simulations, the authors also verified that the growth direction of the nanoplates was related to one of the solvents that worked as a surfactant and its binding affinity to the nucleated particle surface. Debroise et al. [8] studied the impact of $Ca^{2+}$ vacancies and the substitution of $Mg^{2+}$ ions in the altered base structure of protonated β-$(Ca_3PO_4)_2$ (whitlockite type) through DFT techniques and verified that the Ca4 site is more favorable for vacancies. In contrast, the Ca5 site is more prone to be replaced by $Mg^{2+}$ ions.

Altogether, the examples emphasize the applications of Mg-WH as a biomaterial. However, we identified a significant knowledge gap in understanding Mg-WH structure and electrical properties, which can further advance its application in tissue engineering applications, exploring its piezoelectric response. To our knowledge, no theoretical study at the *ab initio* level has reported the structure of Mg-WH from experimental results, nor its electronic properties. In this paper, we employed density functional theory (DFT) methods to understand the structure of whitlockite better and analyze its electronic properties. Also, we synthesized Mg-WH using the coprecipitation method. Later, we characterized it using scanning electron microscopy (SEM-FEG), X-ray diffraction (XRD), and Fourier-transform infrared (FTIR) spectroscopy, comparing our findings with theoretical results.

## 2. Methodology

### 2.1. Computational methods

Quantum Espresso software [20,21] was used to perform the geometry cell optimization of Mg-WH. DFT calculations were carried out using ultrasoft pseudopotentials generated by the Vanderbilt code [22] and employed to represent core-valence electron interactions. The Perdew-Burke-Ernzerhof (PBE) correlation and exchange functional with Generalized Gradient Approximation (GGA) were adopted, considering periodic conditions of the crystal structure. A 2 × 2 × 2 mesh of K-points was generated using the Monkhorst-Pack method, as implemented by the software code. A plane wave basis set was used with cutoffs of 36.75Ry (5 × $10^2$ eV) and 294 Ry (4 × $10^3$ eV) for wave function and charge density, respectively. The bulk was relaxed until the most significant force acting on the atoms was less than 7.35 × $10^{-6}$ Ry/Bohr (0.0001 eV/Å). An accuracy of 7.35 × $10^{-10}$ Ry ($10^{-8}$ eV) was adopted for the electronic convergence of self-consistent calculation.

### 2.2. Experimental methodology

Magnesium whitlockite (Mg-WH) was synthesized using calcium hydroxide ($Ca(OH)_2$, 99.0 %, Dinâmica®), magnesium hydroxide ($Mg(OH)_2$, 95.0 %, Sigma-Aldrich®), and phosphoric acid ($H_3PO_4$, 85.0 %, Sigma-Aldrich®), following a method adapted from Jang et al. [10] and under acidic pH conditions. Briefly, a solution of $Ca(OH)_2$ (0.77 M) and $Mg(OH)_2$ (0.23 M) was mixed in 250 mL of distilled water at 70 °C and continuously stirred for 1 h. A phosphoric acid (0.95 M) solution in 250 mL of distilled water was added dropwise at 2.5 mL/min. The resulting solution was aged at 100 °C for 48 h, aiming for the precipitation of Mg-WH crystals. The precipitate was washed by centrifugation three times (Centrifuge Excelsa® II, Mod. 206 B L, Brazil), lyophilized (Operon Freeze Dryer 55C, South Korea) for 24 h, and calcined at 700 °C for 1 h in an electric furnace (Jung 1612, Brazil).

Characterization of the synthesized Mg-WH powders was performed using X-ray diffraction (XRD) with a diffractometer STADIP S/N 661–0421, employing AgKα radiation (λ = 0.55941 Å), operating at 40 kV and 40 mA. The crystallite size of the nanoparticles was estimated by the Scherrer equation (Eq. (1)). Moreover, Rietveld refinement was performed using GSAS software (https://advancedphotonsource.github.io/GSAS-II-tutorials/) to fit the experimental diffraction pattern with the calculated profile and JCPDS database.

$$D = K\lambda/\beta \cos\theta \quad \text{(Eq. 1)}$$

Where D is the crystallite size of the nanoparticles; K is the Scherrer constant; λ is the wavelength of the X-ray beam; β is the full width at half maximum (FWHM) of the peak, in radians; and θ is the Bragg angle.

Fourier-transform infrared (FTIR) spectra using ATR mode (model SpectrumTwo, PerkinElmer, USA) were recorded at 400-4000 $cm^{-1}$ range (4 $cm^{-1}$ of resolution) to analyze molecular vibrations of phosphate and hydrogen phosphate groups. For the morphological analysis of the surface of the powder, a scanning electron microscope with field emission guns (SEM-FEG) was performed (JSM-IT700HR, JEOL, USA). The chemical composition was evaluated with energy dispersive spectroscopy (EDS).

## 3. Results

To conduct theoretical calculations of the ground state of Mg-WH, we started with the experimental structure reported by Gopal et al. [23]. The optimized structure is displayed in Fig. 1. The crystal unit cell, with a hexagonal structure, belongs to the space group *R*3*c*. Considering the c-axis view (Fig. 1c), $Mg^{2+}$ and $HPO_4^{2-}$ ions alternately compete along three columns: two diagonally and one in the lower left corner (represented by green circles). The optimized data obtained by the simulation

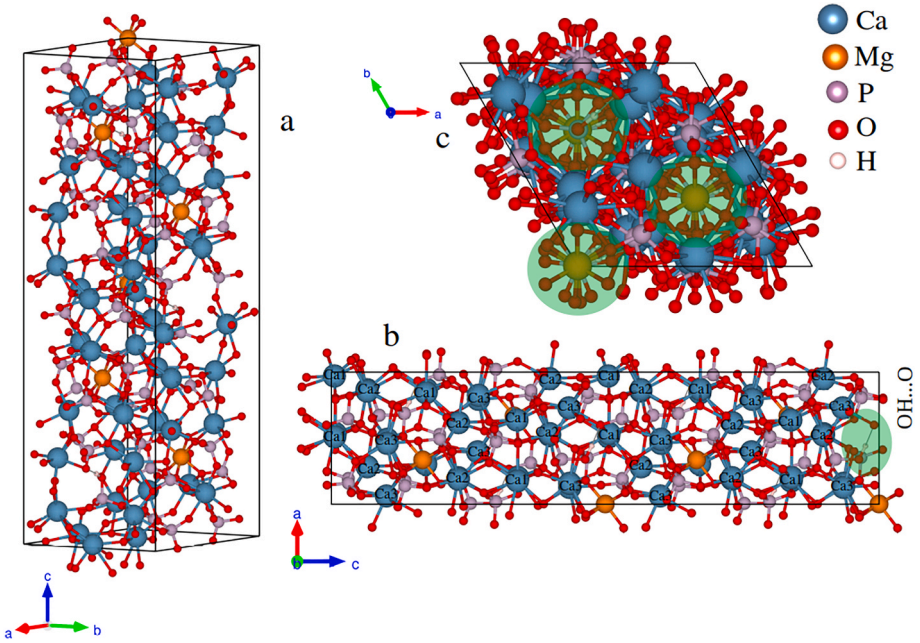


**Fig. 1.** Whitlockite structure (a), and view of the xz (b) and xy (c) planes. The Ca, Mg, P, O, and H atoms colors are, respectively, blue, yellow, light purple, red, and white. The area highlighted in green shows the crystallographic sites where $Mg^{2+}$ and $HPO_4^{2-}$ compete. (For interpretation of the references to color in this figure legend, the reader is referred to the Web version of this article.)

are a = b = 10.4143 Å, c = 37.3992 Å, and a volume of 3512.81 Å$^3$. We also calculated lattice parameters of the synthesized powders by Rietveld refinement and obtained a = b = 10.3358 Å, and c = 37.0856 Å. Such data agrees with the experimental values previously reported [23].

There are three equivalent Ca sites and one Mg site, where eight oxygens coordinate the Ca sites, while the Mg site is coordinated by six oxygens, considering a radius of 3.1 Å (see Fig. S1). The average distances of the Ca-O and Mg-O bonds are described in Table 1.

The cation equivalent site positions are shown in Table 2, compared with those reported for synthetic Mg-WH [23], in fractional positions. There are 18 atoms for each of the Ca equivalent sites and 6 Mg atoms.

Furthermore, the Mg-WH (Fig. 1b) presents a hydrogen bond between the hydrogen atom of $HPO_4^{2-}$ and the oxygen of the neighboring phosphate group, with a length of 1.593 Å, consistent with experimental data reported by Capitelli et al. [19]. The bond distance of the OH group is 1.019 Å, which is in good agreement with the reported data of 1.03 Å [24]. Moreover, a length of 2.61 Å between the oxygen atom of OH and the neighboring oxygen involved in the hydrogen bond was verified, and these three atoms formed a bond angle of 174.8°.

Fig. 2 presents the X-ray diffraction pattern generated by the theoretical model, which was compared with the diffraction pattern from the JCPDS database (JCPDS no. 70–2064) and the experimental pattern of the synthesized Mg-WH. Specifically, Fig. 2a shows each pattern over 3°–25°. In contrast, in Fig. 2b, the patterns are over-imposed, aiming to better compare the patterns in the 9°–13° range, which contains the characteristic peaks of whitlockite. An average crystallite size of 40 nm was also obtained. The Rietveld refinement of XRD data of Mg-WH is presented in Fig. 2c, with Rwp = 5.38 and Rexp = 3.45. The results showed a low value of χ 2 (goodness of fit), 2.4, which indicates a high quality refinement.

**Table 1**
The average distance of X-O bonds in coordination region (X = Ca or Mg).

| Site | X-O average distance |
|---|---|
| Ca1 | 2.552 (0.2) Å |
| Ca2 | 2.494 (0.1) Å |
| Ca3 | 2.494 (0.12) Å |
| Mg | 2.086 (0.011) Å |

* in parentheses are standard deviation.

**Table 2**
Fractional positions (x, y, z) of Ca and Mg cation sites in the WH structure. Comparison between our theoretical data and that available in the literature [23].

| Site | Theoretical | Literature [23] |
|---|---|---|
| Ca1 | 0.3056 0.1684 0.6717 | 0.2951 0.1580 0.6720 |
| Ca2 | 0.2831 0.1507 0.5653 | 0.2810 0.1468 0.5648 |
| Ca3 | 0.3960 0.1836 0.7670 | 0.3880 0.1800 0.7676 |
| Mg | 0.0015 0.0030 0.0000 | 0.0000 0.0000 0.0000 |

Fig. 3 presents the FTIR spectra of experimentally obtained Mg-WH. The spectra exhibit bands assigned to phosphate groups consistent with those reported in the literature [15]. The stretching vibration of P–O is observed at 960 cm$^{-1}$, while the asymmetric stretching of $PO_4^{3-}$ appears as a broad range between 1146 cm$^{-1}$ and 932 cm$^{-1}$. A distinct doublet at 602 cm$^{-1}$ and 554 cm$^{-1}$ is also attributed to the bending vibration of crystalline $PO_4$. A peak confirms the presence of $HPO_4^{2-}$ at 924 cm$^{-1}$, which corresponds to P–O–H stretching, indicating the existence of the whitlockite phase.

The Mg-WH was synthesized by the co-precipitation method in an aqueous system and acid environment and then annealed at 700 °C, resulting in submicrometer powders, as shown in Fig. 4a. The powders exhibit a similar morphology of Mg-WH particles found in literature and synthesized by a similar method [9,10]. The EDS spectrum (Fig. 4b) shows the element distribution based on the general image (Fig. 4c) and the elemental color mapping of the species Ca, Mg, and P that compose the Mg-WH.

Fig. 5 presents the band structure obtained by DFT computational simulation. A gap region with a Fermi level close to the valence bands can be observed from this. The area without available energy bands has a direct gap of 5.228 eV. Fig. 6 shows the density of states from atomic orbitals in atoms that constitute Mg-WH and their sum.

The upper graph (Fig. 6) corresponds to the total density of states per electron-volt, considering the total states of all atomic species in the

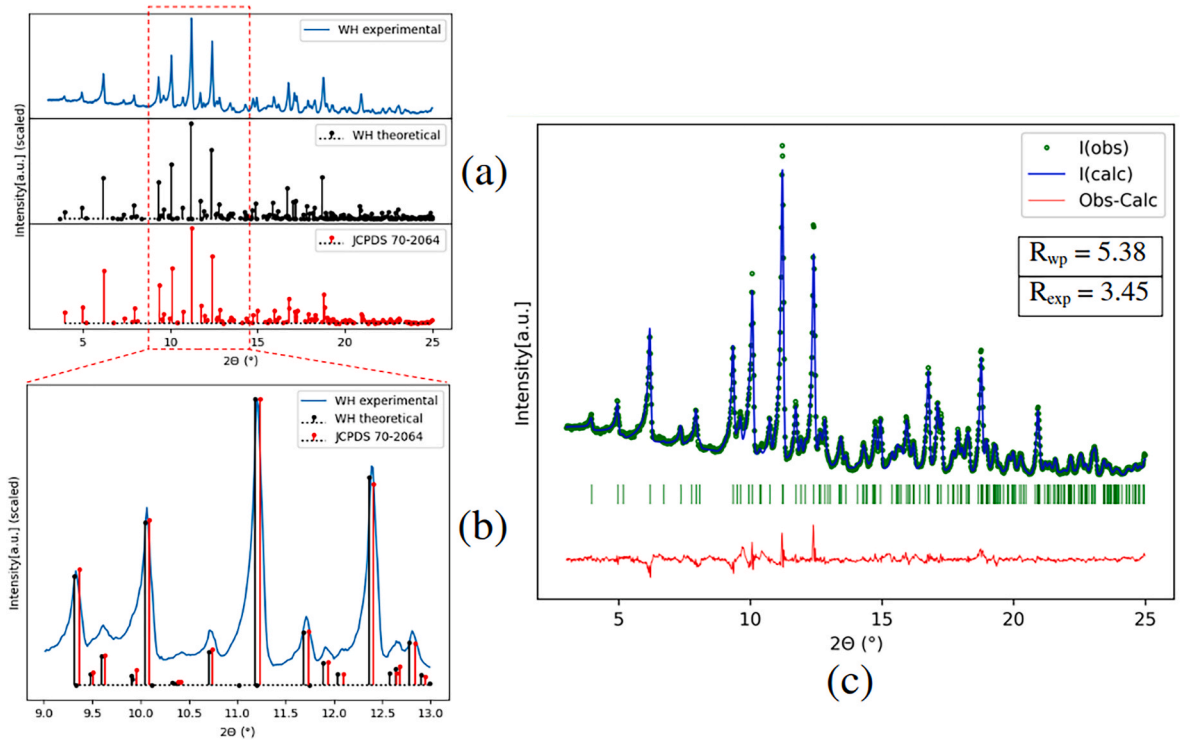


**Fig. 2.** Whitlockite theoretical and experimental XRD pattern. (a) comparison of theoretical, experimental and reference pattern, (b) overlapped patterns at characteristic peaks, and (c) Rietveld refinements of XRD data of Mg-WH synthesized.

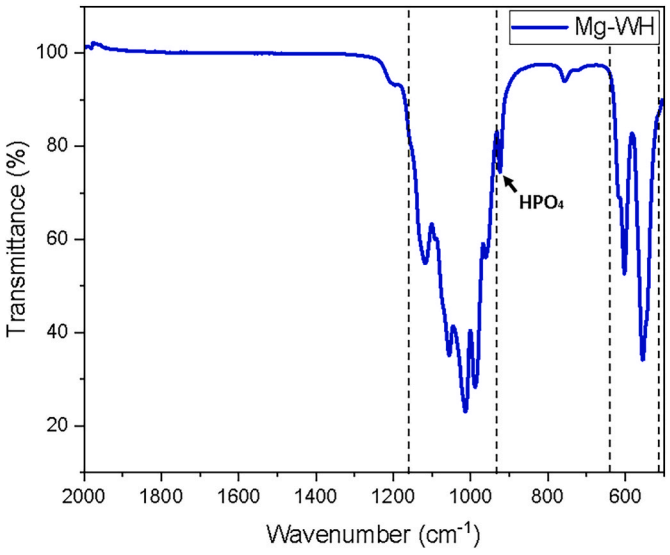


**Fig. 3.** Infrared spectra of synthesized Mg-WH. The dashed lines indicate the characteristic bands of phosphate groups found in the whitlockite phase.

bulk. The other graphs show the contribution of the Ca, H, P, Mg, and O specimens. A shaded region can be observed and corresponds to the sum contribution of orbitals in each atomic species. The left side of the gap region corresponds to occupied levels, and the right side is unoccupied at the ground state.

## 4. Discussion

Among the calcium phosphate ceramics for biological applications, the structure of β-TCP, HAp, and Mg-WH has already been studied by theoretical and experimental researchers [25–31]. However, to the best of our knowledge, we report here for the first time the theoretical model of Mg-WH ($Ca_{18}Mg_2H_2(PO_4)_{14}$) structure using *ab initio* methods. Our results contribute to a better understanding of its structure, aiming to develop new potential materials based on Mg-WH with improved bone tissue repair.

Mg-WH and β-TCP are both resorbable calcium phosphate crystalline phases critical in bone regeneration, and both phases share the same space group, *R*3*c*. The main difference is that Mg-WH has $Mg^{2+}$ and $HPO_4^{2-}$ ions within its structure [8,9,14]. Furthermore, in both bioceramics, the Ca1, Ca2, and Ca3 sites of their crystallographic structure have a similar coordination number for oxygen. In contrast, the Ca5 site has the same coordination number for Mg-WH and β-TCP, occupied by a $Mg^{2+}$ ion in the Mg-WH phase.

In our model, the Ca1 site has a greater average distance and standard deviation (Table 1). After inspecting the distances between oxygen atoms and these sites with a 2.4 Å radius threshold, we verified that Ca1 has three closer O atoms, Ca2 has only one, and Ca3 has two closer O atoms. The magnesium site is located in an approximately octahedral region with a minor average distance. These results bring valuable information for those interested in doping Mg-WH with other elements. Considering the coordination regions of crystallographic sites, we believe the Ca1 site is more susceptible to receiving bigger atoms in substitutional doping of Mg-WH, followed by the Ca2 and Ca3 sites. For smaller atoms, it can be considered the Mg site.

One of the main structural differences between the Mg-WH and β-TCP phases concerns the Ca4 site: it is half occupied in β-TCP and receives the $HPO_4^{2-}$ group in Mg-WH, which forms a strong hydrogen bond. The presence of the hydrogen bonds and $Mg^{2+}$ may play an essential role in the resorbable behavior of Mg-WH in a biological environment [32,33].

Jang et al. [17] reported that the resorbable rate of Mg-WH implants is lower than that of β-TCP implants, which favors enhanced *in vivo* bone regeneration. At the same time, Mg-WH shows an intermediate resorbability compared to HAp and β-TCP. Additionally, Tang et al. [34] reported that whitlockite-type crystals dissolve more slowly than β-TCP,

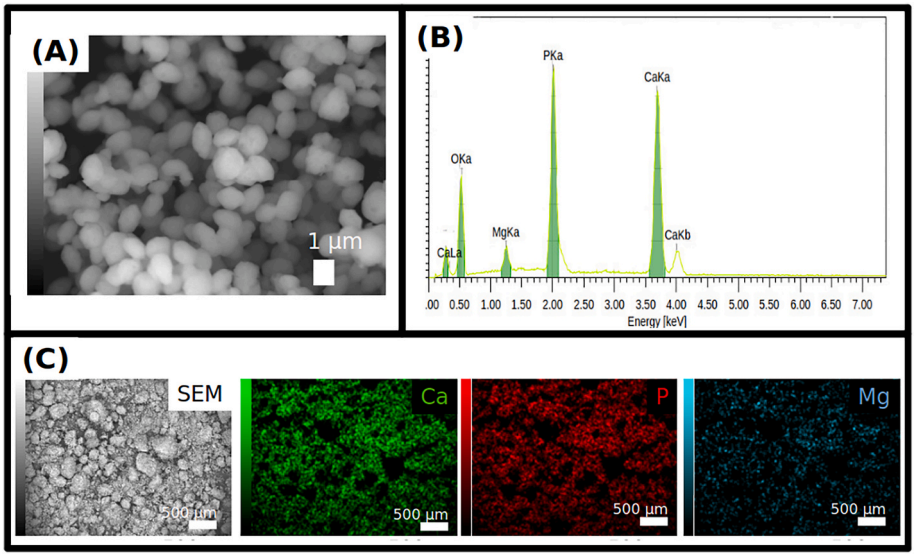


**Fig. 4.** Mg-WH morphological images of (a) FEG-SEM, (b) EDS spectrum, (c) elemental color mapping. (For interpretation of the references to color in this figure legend, the reader is referred to the Web version of this article.)

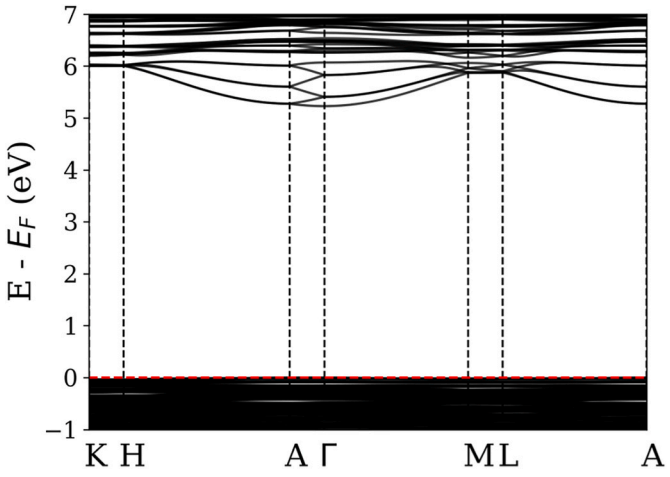


**Fig. 5.** Whitlockite energy band. The Fermi level has been shifted to zero and is represented by the dashed red line. (For interpretation of the references to color in this figure legend, the reader is referred to the Web version of this article.)

and this effect is magnified when more $Mg^{2+}$ ions are added to the composition at the expense of $Ca^{2+}$ ions. This effect was also noticed in other works. Magalhães et al. [35], who synthesized Mg-WH with different $Ca^{2+}/Mg^{2+}$ ratios, showed that the dissolution behavior of Mg-WH relies on the ratio between $Ca^{2+}$, $Mg^{2+}$, and $HPO_4^{2-}$ species within the WH structure [35]. The results shown in our work may be used for further molecular dynamic studies to evaluate the activation energy of dissolution reactions and check whether the Mg2+ or the $HPO_4^{2-}$ sites are required for decreasing the Mg-WH dissolution kinetics, complementing the results found by Magalhães et al. [35]. In other words, more investigation is still needed to understand the key factors involved in the dissolution kinetics of Mg-WH.

Regarding the comparison between the experimental and the *ab initio* XRD diffractograms, there was a slight peak shift of the theoretical XRD pattern compared to reference peaks from JCPDS and the as-prepared material. This shift is due to the approximation of using pseudopotentials for DFT calculations. The theoretical results showed that lattice parameters obtained by the simulation are greater than those of the synthesized Mg-WH in this work and the experiment reported in the literature [23]. This fact caused the displacement of theoretical peaks. Despite that, XRD patterns agree with the synthetic phase produced in our laboratory, validating our simulations.

Complimentarily, FTIR confirms the presence of $HPO_4^{2-}$ in the synthesized material, which is a whitlockite characteristic, evidencing the existence of the aforementioned hydrogen bond.

Based on morphology analysis from SEM-FEG, the smaller Mg-WH particles showed a hexagonal shape, while the bigger particles exhibited a rounded shape, probably due to the annealing process. The SEM-EDS images suggest no formation of other phases, which agrees with the XRD results. Also, EDS mapping shows a uniform presence of elements in the Mg-WH particles without different components, indicating the absence of other impurities.

Regarding the band structure, it can be observed from Fig. 5 that there is a typical gap for ceramic insulators. Besides, the Fermi level is on the highest of the dense top valence bands, indicating a possible tendency to donate electrons. This potential trend can hint at electrical properties that can enhance bone repair. However, further investigation is still needed in this regard.

At first glance, one can see (Fig. 6) that the species type of O(p) contributes the majority to the highest occupied levels, with a minor contribution from Mg(s), and the lowest levels of the conduction band have the main contribution from Mg (s). However, if we carefully inspect, Ca(d) also contributes to the top of occupied levels, and the lowest unoccupied levels also have significant contributions of types Ca (s,d) and O(s). Besides, considering Fermi shifted to 0 eV, all atomic species contribute to DOS from −25 eV to 8 eV. Those ranges with main occupied levels are approximately at −20.7 eV to −16.4 eV and −8.6 eV–0.4 eV. The density of states analysis highlights significant contributions from oxygen and magnesium specimens, with calcium also playing a role near the gap region in conduction and valence bands. These results can support further studies in which the doping of Mg-WH is desired to improve its electrical properties.

By understanding how substitutional doping works in Mg-WH and how Mg and Ca sites influence its bandgap, which was discussed in this article, one can infer that the results of this work may support theoretical and experimental decisions on Mg-WH modification in future works.

## 5. Conclusion

Magnesium whitlockite is an increasingly attractive, promising biomaterial for bone regeneration applications. This study comprehensively analyzes Mg-WH, combining theoretical *ab initio* methods with

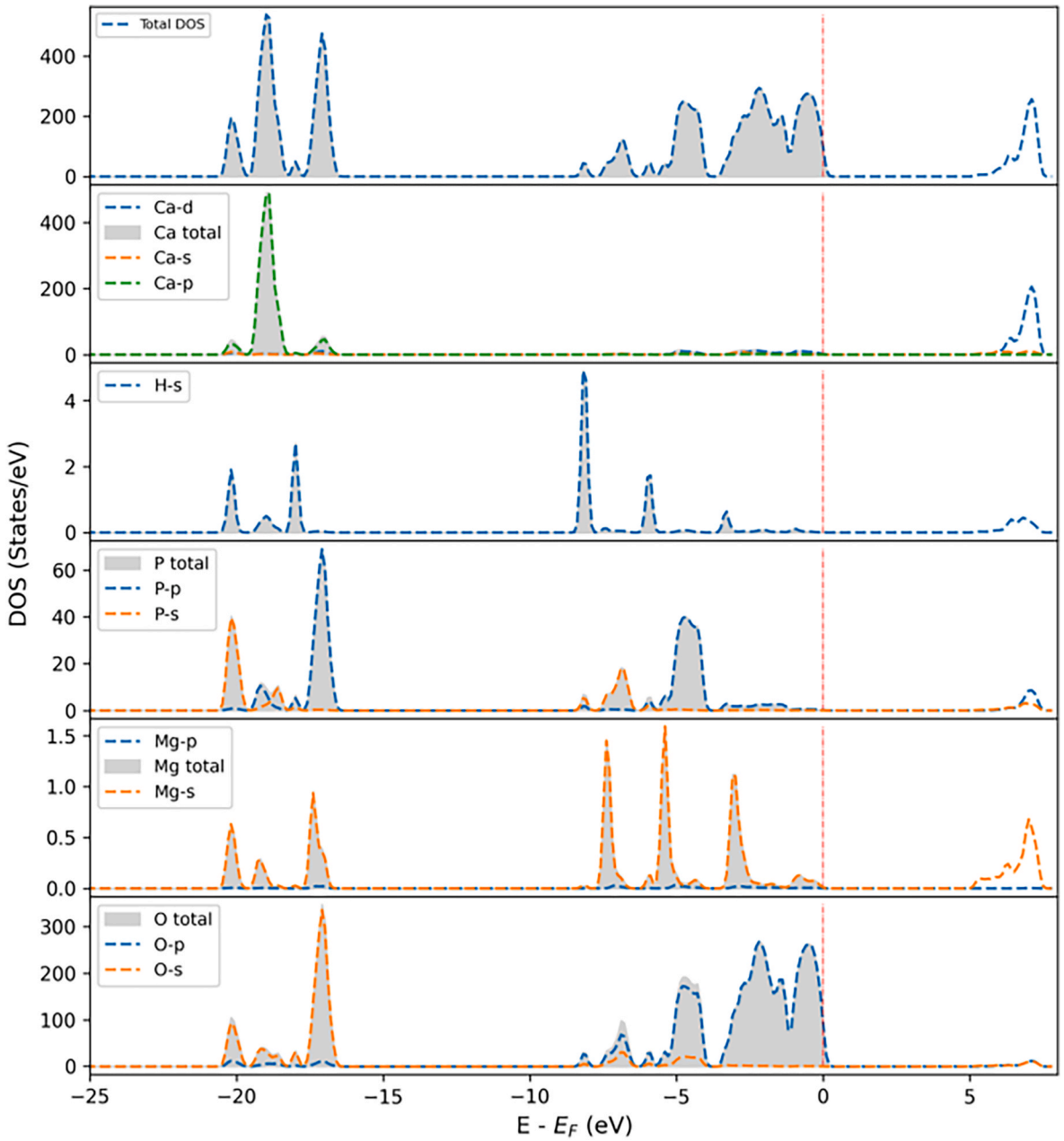


**Fig. 6.** Total density of states and contribution by atomic species. The left side (shaded region) corresponds to valence bands, and the right side of the Fermi level is the conduction bands. The Fermi level has been shifted to zero and is represented by the dashed red line. (For interpretation of the references to color in this figure legend, the reader is referred to the Web version of this article.)

experimental validation. Our results confirm the structural features of Mg-WH. Morphological analysis and XRD patterns are consistent and reveal that the synthesized material exhibits a single whitlockite phase without other phases or impurities. Moreover, the FTIR analysis confirms the presence of hydrogen phosphate in the material, a significant distinction from β-TCP. The model also demonstrated the existence of hydrogen bonds, which may influence the material's interaction under physiological environments. We also showed that the Ca1 site is more likely to be replaced by ions with atomic radii greater than $Mg^{2+}$ in the case of atomic substitution. This research may support future studies on Mg-WH and its potential to improve hard tissue repair.

## CRediT authorship contribution statement

**Emanuel Cleyton Macedo Lemos:** Writing – original draft, Methodology, Investigation, Formal analysis, Data curation, Conceptualization. **Renata Hidemi Moriya:** Investigation, Formal analysis. **Luccas Correa Teruel de Jesus:** Investigation, Formal analysis. **Roger Borges:** Writing – original draft, Investigation, Formal analysis. **Rene de Oliveira:** Validation, Methodology, Investigation, Formal analysis, Data curation. **Nelson Batista de Lima:** Validation, Methodology, Investigation, Formal analysis, Data curation. **Jeverson Teodoro Arantes:** Writing – review & editing, Methodology, Investigation, Formal analysis, Conceptualization. **Juliana Marchi:** Writing – review & editing, Supervision, Resources, Project administration, Investigation, Formal analysis, Conceptualization.

## Declaration of competing interest

The authors declare that they have no known competing financial

interests or personal relationships that could have appeared to influence the work reported in this paper.

## Acknowledgments

The authors thank the financial support of the Federal Institute of Maranhão (IFMA/Brazil) and the Brazilian agencies CNPq/INCT (National Institute of Science and Technology on Materials Informatics, grant n. 371610/2023–0), CAPES (cod 001), CNPq-PIBIC (for LCTJ funding), CNPq (311280/2023–4, JM), and FAPESP (2020/00329–6, JM and 2024/11219–8, JM). The authors acknowledge the computational resources provided by Multiuser Computational Central at the UFABC (CCM/UFABC/Brazil). The experimental facilities at the UFABC, Central Experimental Multiusuário CEM/UFABC, and Centro de Ciência e Tecnologia dos Materiais CECTM/IPEN are also appreciated.

## Appendix A. Supplementary data

Supplementary data to this article can be found online at https://doi.org/10.1016/j.ceramint.2025.05.374.

## References

[1] R. Borges, T. Zambanini, A.M. Pelosine, G.Z. Justo, A.C.S. Souza, Jr. J. Machado, J. F. Schneider, D.R. Araujo, J. Marchil, A colloidal hydrogel-based drug delivery system overcomes the limitation of combining bisphosphonates with bioactive glasses: in vitro evidence of a potential selective bone cancer treatment allied with bone regeneration, Biomaterials Advances 151 (2023) 213441, https://doi.org/10.1016/j.bioadv.2023.213441.

[2] R. Borges, A.M. Pelosine, A.C.S. de Souza, J. Machado, G.Z. Justo, L.F. Gamarra, J. Marchi, Bioactive glasses as carriers of cancer-targeted drugs: challenges and opportunities in bone cancer treatment, Materials (Basel) 15 (2022) 9082, https://doi.org/10.3390/MA15249082, 9082.

[3] K.C. Kai, R. Borges, A.C.F. Pedroni, A.M. Pelosine, M.R. da Cunha, M.M. Marques, D.R. de Araújo, J. Marchi, Tricalcium phosphate-loaded injectable hydrogel as a promising osteogenic and bactericidal teicoplanin-delivery system for osteomyelitis treatment: an in vitro and in vivo investigation, Biomater. Adv. 164 (2024) 213966, https://doi.org/10.1016/j.bioadv.2024.213966.

[4] T. Zambanini, R. Borges, K.C. Kai, J. Marchi, Bioactive glasses for treatment of bone infections, in: K. Gurbinder (Ed.), Biomedical, Therapeutic and Clinical Applications of Bioactive Glasses, first ed., Elsevier, Duxford, 2018, pp. 283–410.

[5] B.M. Brochu, S.R. Sturm, J.A. Kawase De Queiroz Goncalves, N.A. Mirsky, A. I. Sandino, K.Z. Panthaki, K.Z. Panthaki, V.V. Nayak, S. Daunert, L. Witek, P. G. Coelho, Advances in bioceramics for bone regeneration: a narrative review, Biomimetics (New York, N. Y.) 9 (2024), https://doi.org/10.3390/biomimetics9110690.

[6] R. Borges, L.A. Genova, J. Marchi, Microspheres for bone regeneration, in: D.R. de Araujo, L.R. Fraceto (Eds.), Microspheres: Technologies, Applications and Role in Drug Delivery Systems, first ed., Nova Publishers, 2014.

[7] G. Kazakova, T. Safronova, D. Golubchikov, O. Shevtsova, J.V. Rau, Resorbable mg2+-containing phosphates for bone tissue repair, Materials (Basel) 14 (2021), https://doi.org/10.3390/ma14174857.

[8] T. Debroise, E. Colombo, G. Belletti, J. Vekeman, Y. Su, R. Papoular, N.S. Hwang, D. Bazin, M. Daudon, P. Quaino, F. Tielens, One step further in the elucidation of the crystallographic structure of whitlockite, Cryst. Growth Des. 20 (2020) 2553–2561, https://doi.org/10.1021/acs.cgd.9b01679.

[9] H.L. Jang, K. Jin, J. Lee, Y. Kim, S.H. Nahm, K.S. Hong, K.T. Nam, Revisiting whitlockite, the second most abundant biomineral in bone: nanocrystal synthesis in physiologically relevant conditions and biocompatibility evaluation, ACS Nano 8 (2014) 634–641, https://doi.org/10.1021/nn405246h.

[10] H.L. Jang, H.K. Lee, K. Jin, H.-Y. Ahn, H.-E. Lee, K.T. Nam, Phase transformation from hydroxyapatite to the secondary bone mineral, whitlockite, J. Mater. Chem. B 3 (2015) 1342–1349, https://doi.org/10.1039/C4TB01793E.

[11] R. Sasidharan Pillai, V.M. Sglavo, Effect of MgO addition on solid state synthesis and thermal behavior of beta-tricalcium phosphate, Ceram. Int. 41 (2015) 2512–2518, https://doi.org/10.1016/j.ceramint.2014.10.073.

[12] S. Kannan, J.M. Ventura, J.M.F. Ferreira, Aqueous precipitation method for the formation of Mg-stabilized β-tricalcium phosphate: an X-ray diffraction study, Ceram. Int. 33 (2007) 637–641, https://doi.org/10.1016/j.ceramint.2005.11.014.

[13] A. Afonina, A. Dubauskas, V. Klimavicius, A. Zarkov, A. Kareiva, I. Grigoraviciute, Phase transformations during the dissolution-precipitation synthesis of magnesium whitlockite nanopowders from gypsum, Ceram. Int. 49 (2023) 38157–38164, https://doi.org/10.1016/j.ceramint.2023.09.146.

[14] Y. Yang, H. Wang, H. Yang, Y. Zhao, J. Guo, X. Yin, T. Ma, X. Liu, L. Li, Magnesium-based whitlockite bone mineral promotes neural and osteogenic activities, ACS Biomater. Sci. Eng. 6 (2020) 5785–5796, https://doi.org/10.1021/acsbiomaterials.0c00852.

[15] V.K. Kaliannagounder, N.P.M.J. Raj, A.R. Unnithan, J. Park, S.S. Park, S.J. Kim, C. H. Park, C.S. Kim, A.R.K. Sasikala, Remotely controlled self-powering electrical stimulators for osteogenic differentiation using bone inspired bioactive piezoelectric whitlockite nanoparticles, Nano Energy 85 (2021), https://doi.org/10.1016/j.nanoen.2021.105901.

[16] M. Kamitakahara, C. Ohtsuki, T. Miyazaki, Review paper: behavior of ceramic biomaterials derived from tricalcium phosphate in physiological condition, J. Biomater. Appl. 23 (2008) 197–212, https://doi.org/10.1177/0885328208096798.

[17] H.L. Jang, G Bin Zheng, J. Park, H.D. Kim, H.-R. Baek, H.K. Lee, K. Lee, H.N. Han, C.-K. Lee, N.S. Hwang, J.H. Lee, K.T. Nam, In vitro and in vivo evaluation of whitlockite biocompatibility: comparative study with hydroxyapatite and β-Tricalcium phosphate, Adv. Healthcare Mater. 5 (2016) 128–136, https://doi.org/10.1002/adhm.201400824.

[18] C. Qi, Y.-J. Zhu, F. Chen, J. Wu, Porous microspheres of magnesium whitlockite and amorphous calcium magnesium phosphate: microwave-assisted rapid synthesis using creatine phosphate, and application in drug delivery, J. Mater. Chem. B 3 (2015) 7775–7786, https://doi.org/10.1039/C5TB01106J.

[19] C. Wang, K.-J. Jeong, H.J. Park, M. Lee, S.-C. Ryu, D.Y. Hwang, K.H. Nam, I. H. Han, J. Lee, Synthesis and formation mechanism of bone mineral, whitlockite nanocrystals in tri-solvent system, J. Colloid Interface Sci. 569 (2020) 1–11, https://doi.org/10.1016/j.jcis.2020.02.072.

[20] P. Giannozzi, O. Andreussi, T. Brumme, O. Bunau, M.B.N. Calandra, R. Car, C. Cavazzoni, D. Ceresoli, M. Cococcioni, N.C. Carnimeo, A.D. Corso, S. de Gironcoli, P. Delugas, R.A.D. Jr, A.F. Floris, G. Fratesi, G. Fugallo, R. Gebauer, U. Gerstmann, F. Giustino, T.G. Jia, M. Kawamura, H.-Y. Ko, A. Kokalj, E. Küçükbenli, M. Lazzeri, M.M. Marzari, F. Mauri, N.L. Nguyen, H.-V. Nguyen, A. Otero-de-la-Roza, L.P. Poncé, D. Rocca, R. Sabatini, B. Santra, M. Schlipf, A.P. S. Smogunov, I. Timrov, T. Thonhauser, P. Umari, N. Vast, X. Wu, S. Baroni, Advanced capabilities for materials modelling with QUANTUM ESPRESSO, J. Phys. Condens. Matter 29 (2017) 465901.

[21] P. Giannozzi, S. Baroni, N. Bonini, M. Calandra, R.C. Cavazzoni, D. Ceresoli, G. L. Chiarotti, M. Cococcioni, I.D. Dal Corso, S. de Gironcoli, S. Fabris, G. Fratesi, R. G. Gerstmann, C. Gougoussis, A. Kokalj, M. Lazzeri, L.M.-S. Marzari, F. Mauri, R. Mazzarello, S. Paolini, A.P. Paulatto, C. Sbraccia, S. Scandolo, G. Sclauzero, A.P. S. Smogunov, P. Umari, R.M. Wentzcovitch, QUANTUM ESPRESSO: a modular and open-source software project for quantum simulations of materials, J. Phys. Condens. Matter 21 (19pp) (2009) 395502.

[22] K.F. Garrity, J.W. Bennett, K.M. Rabe, D. Vanderbilt, Pseudopotentials for high-throughput DFT calculations, Comput. Mater. Sci. 81 (2014) 446–452, https://doi.org/10.1016/j.commatsci.2013.08.053.

[23] R. Gopal, C. Calvo, J. Ito, W.K. Sabine, Crystal structure of synthetic Mg-Whitlockite, Ca18Mg2H2(PO4)14, Can. J. Chem. 52 (1974) 1155–1164, https://doi.org/10.1139/v74-181.

[24] F. Capitelli, F. Bosi, S.C. Capelli, F. Radica, G Della Ventura, Neutron and xrd single-crystal diffraction study and vibrational properties of whitlockite, the natural counterpart of synthetic tricalcium phosphate, Crystals (Basel) 11 (2021) 1–19, https://doi.org/10.3390/cryst11030225.

[25] B. Sahin, T. Ates, I.K. Acari, A.A. Barzinjy, B. Ates, İ. Özcan, N. Bulut, S. Keser, O. Kaygili, Tuning electronic properties of hydroxyapatite through controlled doping using zinc, silver, and praseodymium: a density of states and experimental study, Ceram. Int. 50 (2024) 7919–7929, https://doi.org/10.1016/j.ceramint.2023.12.120.

[26] A.Z. Alshemary, Y.F. Goh, I. Shakir, R. Hussain, Synthesis, characterization and optical properties of chromium doped β-Tricalcium phosphate, Ceram. Int. 41 (2015) 1663–1669, https://doi.org/10.1016/j.ceramint.2014.09.107.

[27] M.H. Kebiroglu, C. Orek, N. Bulut, O. Kaygili, S. Keser, T. Ates, Temperature dependent structural and vibrational properties of hydroxyapatite: a theoretical and experimental study, Ceram. Int. 43 (2017) 15899–15904, https://doi.org/10.1016/j.ceramint.2017.08.164.

[28] V.S. Bystrov, E.V. Paramonova, A.V. Bystrova, L.A. Avakyan, N.V. Bulina, Structural and physical properties of Sr/Ca and Mg/Ca substituted hydroxyapatite: modeling and experiments, Ferroelectrics 590 (2022) 41–48, https://doi.org/10.1080/00150193.2022.2037937.

[29] D.C. Garcia, L.E. Mingrone, de Sá MJC, Evaluation of osseointegration and bone healing using pure-phase β - TCP ceramic implant in bone critical defects. A systematic review, Front. Vet. Sci. 9 (2022), https://doi.org/10.3389/fvets.2022.859920.

[30] V.G. DileepKumar, M.S. Sridhar, P. Aramwit, V.K. Krut'ko, O.N. Musskaya, I. E. Glazov, N. Reddy, A review on the synthesis and properties of hydroxyapatite for biomedical applications, J. Biomater. Sci. Polym. Ed. 33 (2022) 229–261, https://doi.org/10.1080/09205063.2021.1980985.

[31] Q. Liu, J.H. Kim, M. Cho, S.H. Kim, B. Xu, S. Amirthalingam, N.S. Hwang, J.H. Lee, Bioactive magnesium-based whitlockite ceramic as bone cement additives for enhancing osseointegration and bone regeneration, Mater. Des. 229 (2023) 111914, https://doi.org/10.1016/j.matdes.2023.111914.

[32] D.N. Misra, Adsorption on hydroxyapatite: role of hydrogen bonding and interphase coupling, Langmuir 4 (1988) 953–958, https://doi.org/10.1021/la00082a029.

[33] G.S.D. King, Hydrogen bonds in crystals, in: P.L. Huyskens, W.A.P. Luck, T. Zeegers-Huyskens (Eds.), Intermolecular Forces: an Introduction to Modern Methods and Results, Springer Berlin Heidelberg, Berlin, Heidelberg, 1991, pp. 451–458, https://doi.org/10.1007/978-3-642-76260-4_20.

[34] R. Tang, W. Wu, M. Haas, G.H. Nancollas, Kinetics of dissolution of β-Tricalcium phosphate, Langmuir 17 (2001) 3480–3485, https://doi.org/10.1021/la001730n.

[35] M.C.F. Magalhães, M.O.G. Costa, On the solubility of whitlockite, Ca9Mg(HPO4)(PO4)6, in aqueous solution at 298.15 K, Monatsh. Chem. 149 (2018) 253–260, https://doi.org/10.1007/s00706-017-2129-z.